Laser and Particle Beams (2016), *34*, 562–566.

doi:10.1017/S0263034616000471

Improvement of proton beam quality by an optimized dragging field generated by the ultraintense laser interactions with a complex double-layer target

F. J. WU,[1] L. Q. SHAN,[2] W. M. ZHOU,[2] T. DUAN,[1] Y. L. JI,[1] C. R. WU,[1] J. L. JIAO,[2] Z. M. ZHANG,[2] AND Y. Q. GU[2]

[1]Joint Laboratory for Extreme Conditions Matter Properties, Southwest University of Science and Technology, Mianyang, Sichuan, People's Republic of China
[2]Science and Technology on Plasma Physics Laboratory, Research Center of Laser Fusion, China Academy of Engineering Physics, Mianyang, Sichuan, People's Republic of China

(Received 23 May 2016; Accepted 7 July 2016)

Abstract

A scheme for the improvement of proton beam quality by the optimized dragging field from the interaction of ultraintense laser pulse with a complex double-layer target is proposed and demonstrated by one-dimensional particle-in-cell (Opic1D) simulations. The complex double-layer target consists of an overdense proton thin foil followed by a mixed hydrocarbon (CH) underdense plasma. Because of the existence of carbon ions, the dragging field in the mixed CH underdense plasma becomes stronger and flatter in the location of the proton beam than that in a pure hydrogen (H) underdense plasma. The optimized dragging field can keep trapping and accelerating protons in the mixed CH underdense target to high quality. Consequently, the energy spread of the proton beam in the mixed CH underdense plasma can be greatly reduced down to 2.6% and average energy of protons can reach to 9 GeV with circularly polarized lasers at intensities 2.74×10^{22} W/cm^2.

Keywords: Laser–plasma interaction; Complex double-layer target; Optimized dragging field; Proton acceleration; PIC simulation

1. INTRODUCTION

In recent years, ion acceleration from the interaction of an ultraintense laser pusle with plasma has attracted wide attention (Zhou *et al*., 2010; Macchi *et al*., 2013; Wu *et al*., 2013). The generated ion beams have many potential applications, including fast ignition of inertial confinement fusion (Roth *et al*., 2001), cancer therapy (Ledingham *et al*., 2014), laser nuclear physics (Borghesi *et al*., 2006), high-resolution radiography (Paudel *et al*., 2012), and so on. Most of these applications require high-quality ion beams with high conversion efficiency, a large particle number and low energy spread, etc. (Macchi *et al*., 2013).

Radiation pressure acceleration (RPA) has been considered as a promising scheme to produce high-quality ion beams suitable for many applications. According to the target thickness, usually there are two distinct modes of RPA mechanisms: (light sail) LS-RPA for thin target (Yan *et al*., 2008; Chen *et al*., 2009; Qiao *et al*., 2010; Yu *et al*., 2010; Kar *et al*., 2012; Palmer *et al*., 2012; Pae *et al*., 2016) and (hole-boring) HB-RPA for the thick target (Robinson *et al*., 2009; Zhang *et al*., 2011; Weng *et al*., 2015, 2016). In particular, HB-RPA has the potential to generate energetic ion beams with large particle number (Badziak *et al*., 2011; Weng *et al*., 2016). In the HB-RPA regime, the ponderomotive force of laser pulse drives the local electrons inward, resulting in a shock-like double-layer region with large charge separation field. The latter could trap and reflect the ions initially located ahead of the double layer to a speed twice of the shock velocity, accelerating them like a piston (Schlegel *et al*., 2009). When the piston is detached from the target and further accelerated as a whole by the radiation pressure, the acceleration stage is called LS-RPA. Recently, Ji *et al*. presented that the laser-driven foil in the LS-RPA stage can serve as a perfect relativistic piston, which can trap and reflect the protons in underdense plasma to higher energies than foil protons in the simple LS-RPA regime (Ji *et al*., 2014). However, the dragging field behind the foil increases verse distance,

Address correspondence and reprint requests to: Y. Q. Gu, Science and Technology on Plasma Physics Laboratory, Research Center of Laser Fusion, China Academy of Engineering Physics, Mianyang, Sichuan, People's Republic of China. E-mail: yqgu@caep.cn

and it will lead to the protons defocus in phase space and broaden its energy spectrum. Of course, quasi-monoenergetic proton beams can be achieved by reducing the plasma length (Ji *et al.*, 2014). Moreover, we can optimize the dragging field to further improve the quality of the proton beam accelerated by the relativistic piston.

In this paper, we present a complex double-layer target that is illuminated by a circularly polarized (CP) laser pulse to generate an optimized dragging field. The complex double-layer target is composed of an overdense proton thin foil followed by a mixed hydrocarbon (CH) underdense plasma region. Much work has shown that using mixed CH targets can effectively alleviate transverse instabilities and reduce the energy spread of proton beam in the RPA mechanism (Yu *et al.*, 2010; Kar *et al.*, 2012; Pae *et al.*, 2016). The mixed CH underdense plasma employed here is to produce an optimized dragging field, which can trap and accelerate the protons to high quality. The thin foil target is first accelerated by the light pressure as a whole in the simple LS-RPA regime, and a moving electrostatic field generated by the thin foil can serve as the relativistic piston. As the piston propagates into the mixed CH underdense plasma region, it can trap and reflect the protons to ultrahigh energies with low energy spread. The existence of carbon ions can effectively optimize the dragging field behind the piston in mixed CH underdense plasma, and so the optimized dragging field decreases more slowly than that of the pure hydrogen (H) target. As a result, the protons in the mixed CH underdense plasma are trapped and accelerated by a slightly uniform strong electrostatic field. It is demonstrated by one-dimensional relativistic particle-in-cell (PIC) simulations.

2. PIC SIMULATION MODEL

This paper presents numerical results obtained by one-dimensional relativistic PIC Opic1D (Zhang *et al.*, 2014) to avoid multidimensional effects. The simulations are performed for a CP laser pulse with peak amplitude $a = 100$ (corresponding to the intensity 2.74×10^{22} W/cm^2) and laser wavelength $\lambda = 1$ μm. The laser pulse shape is described by a trapezoidal. Its amplitude increases linearly to the maximum in 1 T (T is the laser period) and then remains constant for 50 T. Initial electron density distribution of the complex double-layer target is shown in Figure 1. The electron density of the overdense proton thin foil is $n_{e1} = 80\ n_c$ (black line), where $n_c = \omega^2 m_e / 4\pi e^2$ is the critical density for the corresponding incident laser pulse, and m_e, e, ω represent the electron mass, electron charge, and the laser frequency, respectively. The proton density of the thin foil is the same as electron density $n_{p1} = 80\ n_c$. The foil thickness is $d_f = 0.4\ \lambda$, which corresponds to the optimal LS-RPA condition (Macchi *et al.*, 2009). The mixed CH underdense plasma is composed of carbon ions (C^{6+}) and protons (H) with the same density $0.014\ n_c$ ($n_C : n_{p2} = 1{:}1$), which corresponds to an electron density $n_{e2} = 0.1\ n_c$ (red line). The thickness of the mixed CH underdense plasma is $D = 10\ \lambda$. The foil target is initially

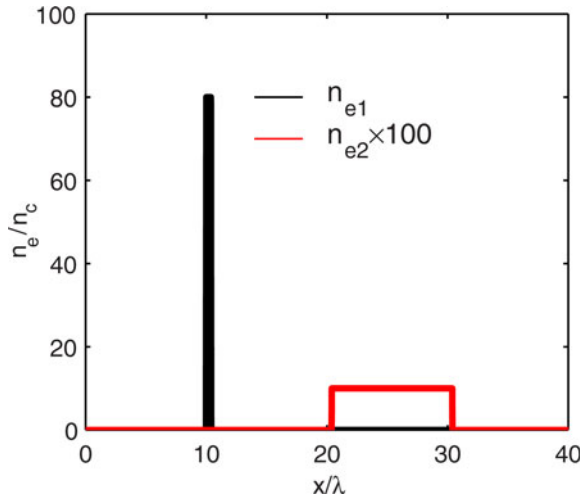

Fig. 1. Initial electron density distribution of the complex double-layer target.

located at 10 λ and the wave front of the laser pulse impinges on its surface at $t = 10$ T. The distance between the foil and underdense plasma is 10 λ. The simulation box size is 500 λ with mesh grid 50,000 in the x-direction. Each cell of the foil target is filled up with 1000 macroparticles and the underdense plasma with 100 macroparticles. The initial electron and ion temperatures are both set to zeros. For comparison, we calculate a pure H underdense plasma with the same thickness, location, and electron density $n_{e2} = 0.1\ n_c$.

3. SIMULATION RESULTS

We have applied one-dimensional PIC Opic1D, where transverse nonuniformity of the laser and the target and transverse instabilities of the target during acceleration process are ignored. In Figure 2, we show the spatial distribution of laser field, electrostatic field, electron density, proton density, and carbon ion density from PIC simulation at: (a) $t =$ 11 T, (b) $t = 35$ T, (c) $t = 100$ T, and (d) $t = 300$ T, respectively. The electron density is shown as negative to show the different densities of the ions and electrons more clearly.

In Figure 2a at $t = 11$ T, the electrons in the foil are first pushed by the steady ponderomotive force of ultraintense CP laser pulses and quickly compressed in a very thin layer at the front of laser pulse, then the protons in the foil are pulled by the induced strong charge separation electrostatic field E_x. Subsequently, the protons and electrons in the foil are pushed forward as a piston by the laser radiation pressure in the LS-RPA regime. Figure 2b shows that the moving piston driven by intense laser pulses propagates into the mixed CH underdense plasma region, the electrons in underdense plasma are also quickly compressed into a thin layer at the laser front. Since carbons and protons in underdense plasma are initially colocated, the protons experience an earlier trapping and reflecting due to their higher charge-to-mass ratio (Z_i/m_i) by the moving piston (Qiao

https://doi.org/10.1017/S0263034616000471 Published online by Cambridge University Press

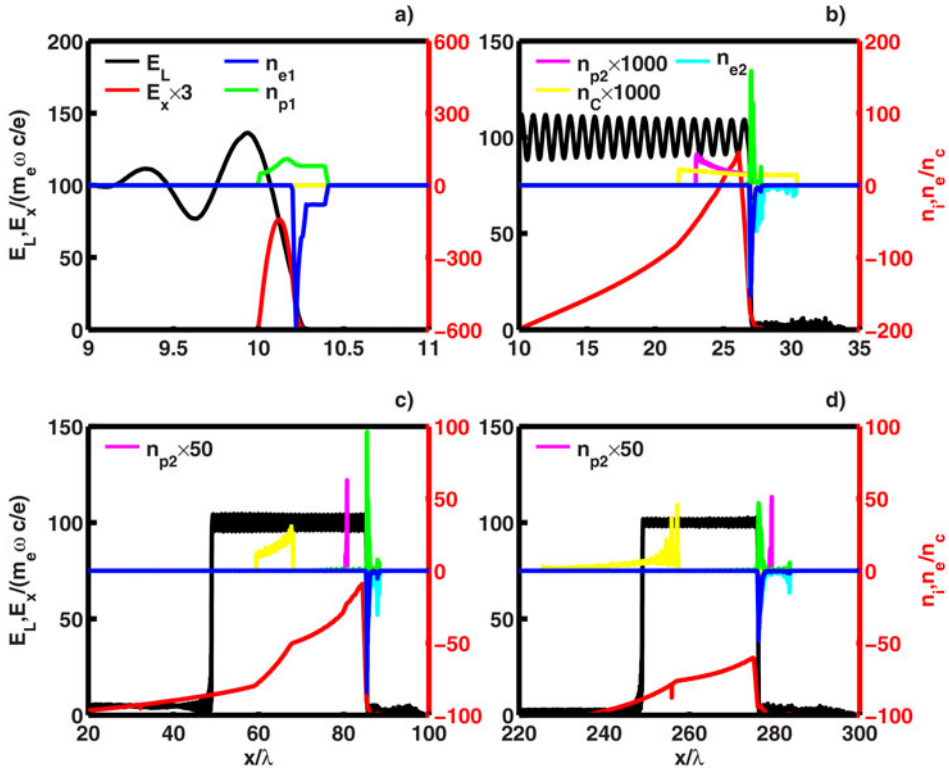

Fig. 2. Spatial distribution of the laser field $E_L = \sqrt{E_y^2 + E_z^2}$ (black line), electrostatic field E_x (red line), electron density n_{e1}/n_c (blue line) and proton density n_{p1}/n_c (green line) in the foil for the mixed CH underdense plasma at four times; (a) $t = 11$ T, (b) $t = 35$ T, (c) $t = 100$ T, and (d) $t = 300$ T, respectively. The spatial density distribution of electrons n_{e2}/n_c (cyan line) and protons n_{p2}/n_c (magenta line) as well as carbon ions n_C/n_c (yellow line) in the mixed CH underdense plasma are also shown.

et al, 2010; Yu *et al*., 2010), while the heavier carbon ions are almost unaffected at $t = 35$ T. The dragging field behind the foil drops almost linearly with the distance. At $t = 100$ T as shown in Figure 2c, the dragging field is optimized due to the existence of carbon ions, and the optimized field behind the piston drops with distance more slowly than that in Figure 2b. These two ions in the mixed CH underdense plasma experience clearly different dragging field. Most of all, the trapped protons experience a stronger and slightly flat dragging field, whereas the carbon ions feel a weaker and defocused field. As a result, the distance between the two ions in space increases. The proton beam is accelerated to high velocity with a small size and carbon ions are spread widely in space. Figure 2d shows that the protons in the mixed CH underdense plasma have surpassed the relativistic piston structure, as the velocity of the foil reaches the critical value at $t = 300$ T. Thereafter, the protons will not be trapped any more, and their energy will get saturated. The carbon ions are extensively spread in space and do not form a clear bunch. During the whole process, a portion of laser is consumed in the interaction and the peak amplitude of the dragging field gradually decreases with time, which is consistent with a previous paper (Ji *et al*., 2014).

Figure 3a, 3b show the temporal evolution of average energy and energy spectra for protons in the mixed CH underdense target, the pure H underdense target, and the thin foil target, respectively. Since the laser pulse is firstly incident onto the thin foil target, the average energy of proton in the foil is larger than that in other two cases before $t =$ 70 T. Subsequently, the average energy of trapped and reflected protons by the dragging field in underdense plasma is much higher than that of thin foil targets. At $t = 300$ T, the proton average energy in the mixed CH target is as high as 9 GeV, which is slightly higher than that in the pure H target and nearly three times as much as that of the thin foil in a simple LS-RPA mechanism. It is clear that using mixed CH underdense plasma can effectively increase the average energy of the protons. In Figure 3b, the energy spectra of different cases show that the proton energy increases more in underdense plasma than that of thin foil in the simple LS-RPA regime. Moreover, the energy spread E/E_{FWHM} is only 2.6% in the mixed CH case, whereas that in the pure H case and thin foil is about 15.8 and 8.5%, respectively. The result clearly indicates that using a mixed CH underdense target can significantly improve the average energy and energy spread of the proton beam.

The improvement of proton beam quality in the mixed CH underdense plasma can be explained by the electrostatic field E_x as shown in Figure 4a. For comparison, Figure 4b shows the electrostatic field in a pure H underdense plasma case. The insets show the spatial distribution of E_x and ion density n_i at $t = 100$ T in both the cases. Although the peak value of

https://doi.org/10.1017/S0263034616000471 Published online by Cambridge University Press

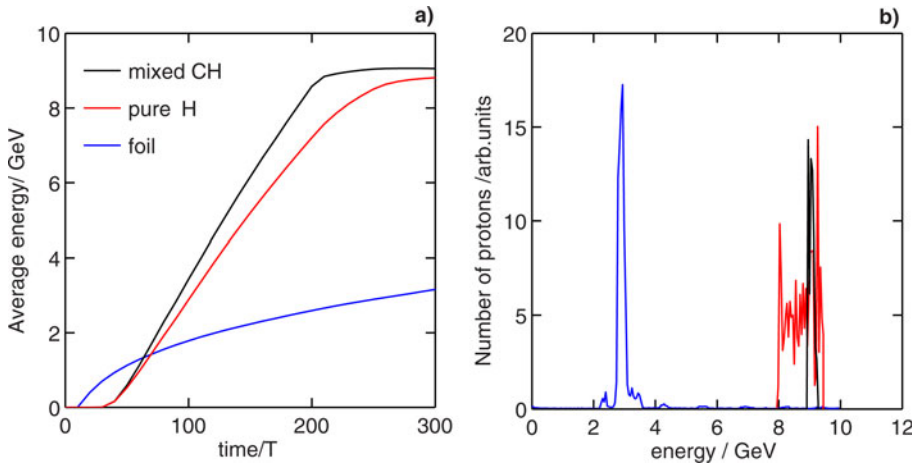

Fig. 3. (a) Temporal evolution of proton average energy and (b) energy spectra of protons at $t =$ 300 T. The black line means the mixed CH underdense plasma, and the red and blue lines are for the pure H underdense plasma and the thin foil, respectively.

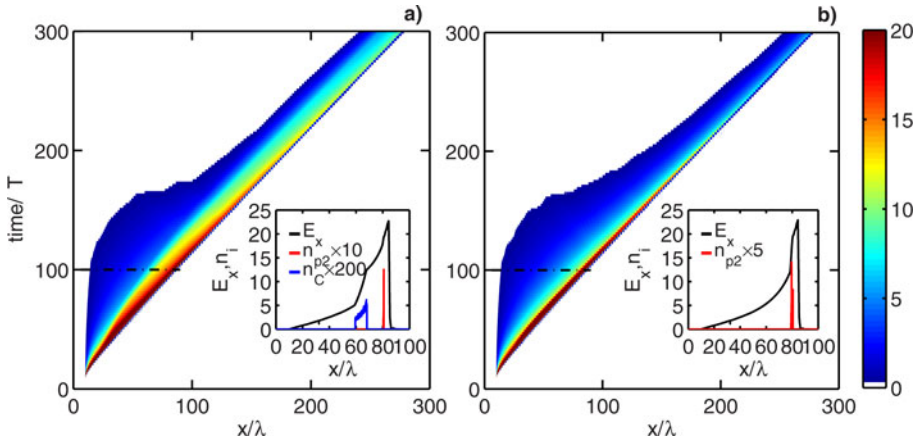

Fig. 4. Spatial–temporal of the electrostatic field E_x from 1D simulation for (a) the mixed CH target and (b) the pure H target. The insets show the spatial distribution of protons (red line) and carbon ions (blue line) density and electrostatic field E_x (black line) corresponding to the the dashed black lines at $t = 100$ T.

E_x in the inset for both targets is almost the same at the same time, there is a distinctive difference in the slope of dragging field. The dragging field in the mixed CH target becomes stronger and flatter in the location of the proton beam than that in the pure H target. During the whole process, the protons in the mixed CH underdense plasma are located at the optimized dragging field, which leads to the compact proton beam structure and the carbon ions spread extensively in space in Figure 4a. For the pure H target case, the protons are located at the quickly decreased part of the dragging field, which results in the protons defocusing in phase space.

4. CONCLUSION

In conclusion, we investigated an optimization of the dragging field in the interaction of the ultraintense CP laser pulse with the complex double target using 1D PIC simulations. Due to presence of the carbon ions in mixed CH underdense plasma, the dragging field is optimized and the quality of proton beam is significantly improved. The proton average energy in the mixed CH target can reach to 9 GeV, which is slightly higher than that in the pure H target and nearly three times as much as that of the thin foil in simple LS-RPA mechanism. Moreover, the proton energy spread of the mixed CH case is only 2.6%, while that in the pure H case and thin foil is about 15.8 and 8.5%, respectively. The studies of the CH ratio of the mixed underdense plasma and 2D PIC sumulations have been also investigated and the results will be presented in future publication.

ACKNOWLEDGMENTS

This work is supported by the Natural Science Foundation of China (Grant numbers 11305157 and 11405141) and the Research Foundation for the Doctor of Southwest University of Science and Technology (Grant number 10ZX7127).

https://doi.org/10.1017/S0263034616000471 Published online by Cambridge University Press

REFERENCES

Badziak, J., Mishra, G., Gupta, N.K. & Holkundkar, A.R. (2011). Generation of ultraintense proton beams by multi-ps circularly polarized laser pulses for fast ignition-related applications. *Phys. Plasma* **18**, 053108.

Borghesi, M., Fuchs, J., Bulanov, S.V., Mackinnon, A.J., Patel, P.K. & Roth, M. (2006). Fast ion generation by high-intensity laser irradiation of solid targets and applications. *Fusion. Sci. Technol*. **49**, 412–439.

Chen, M., Pukhov, A., Yu, T.P. & Sheng, Z.M. (2009). Enhanced collimated GeV monoenergetic ion acceleration from a shaped foil target irradiated by a circularly polarized laser pulse. *Phys. Rev. Lett*. **103**, 024801.

Ji, L.L., Pukhov, A. & Shen, B.F. (2014). Ion acceleration in the 'dragging field' of a light–pressure-driven piston. *New J. Phys*. **16**, 063047.

Kar, S., Kakolee, K.F., Qiao, B., Macchi, A., Cerchez, M., Doria, D., Geissler, M., McKenna, P., Neely, D., Osterholz, J., Prasad, R., Quinn, K., Ramakrishna, B., Sarri, G., Willi, O., Yuan, X.Y., Zepf, M. & Borghesi, M. (2012). Ion acceleration in multispecies targets driven by intense laser radiation pressure. *Phys. Rev. Lett*. **109**, 185006.

Ledingham, K.W.D., Bolton, P.R., Shikazono, N. & Ma, C.M. (2014). Towards laser driven hadron cancer radiotherapy: A review of progress. *Appl. Sci*. **4**, 402–443.

Macchi, A., Borghesi, M. & Passoni, M. (2013). Ion acceleration by superintense laser–plasma interaction. *Rev. Mod. Phys*. **85**, 751–793.

Macchi, A., Veghini, S. & Pegoraro, F. (2009). "Light sail" acceleration reexamined. *Phys. Rev. Lett*. **103**, 085003.

Pae, K.H., Kim, C.M. & Nam, C.H. (2016). Generation of quasi-monoenergetic protons from a double-species target driven by the radiation pressure of an ultraintense laser pulse. *Phys. Plasma* **23**, 033117.

Palmer, C.A.J., Schreiber, J., Nagel, S.R., Dover, N.P., Bellei, C., Beg, F.N., Bott, S., Clarke, R.J., Dangor, A.E., Hassan, S.M., Hilz, P., Jung, D., Kneip, S., Mangles, S.P.D., Lancaster, K.L., Rehman, A., Robinson, A.P.L., Spindloe, C., Szerypo, J., Tatarakis, M., Yeung, M., Zepf, M. & Najmudin, Z. (2012). Rayleigh–Taylor instability of an ultrathin foil accelerated by the radiation pressure of an intense laser. *Phys. Rev. Lett*. **108**, 225002.

Paudel, Y., Renard-Le Galloudec, N., Nicolai, Ph., d'Humieres, E., Faenov, Ya., Kantsyrev, V.L., Safronova, A.S., Shrestha, I., Osborne, G.C., Shlyaptseva, V.V. & Sentoku, Y. (2012). Self-proton/ion radiography of laser-produced proton/ion beam from thin foil targets. *Phys. Plasma* **19**, 123101.

Qiao, B., Zepf, M., Borghesi, M., Dromey, B., Geissler, M., Karmakar, A. & Gibbon, P. (2010). Radiation-pressure acceleration of ion beams from nanofoil targets: The leaky light-sail regime. *Phys. Rev. Lett*. **105**, 155002.

Robinson, A.P.L., Gibbon, P., Zepf, M., Kar, S., Evans, R.G. & Bellei, C. (2009). Relativistically correct hole-boring and ion acceleration by circularly polarized laser pulses. *Plasma Phys. Control. Fusion* **51**, 024004.

Roth, M., Cowan, T.E., Key, M.H., Hatchett, S.P., Brown, C., Fountain, W., Johnson, J., Pennington, D.M., Snavely, R.A., Wilks, S.C., Yasuike, K., Ruhl, H., Pegoraro, F., Bulanov, S.V., Campbell, E.M., Perry, M.D. & Powell, H. (2001). Fast ignition by intense laser-accelerated proton beams. *Phys. Rev. Lett*. **86**, 436–439.

Schlegel, T., Naumova, N., Tikhonchuk, V.T., Labaune, C., Sokolov, I.V. & Mourou, G. (2009). Relativistic laser piston model: Ponderomotive ion acceleration in dense plasmas using ultraintense laser pulses. *Phys. Plasma* **16**, 083103.

Weng, S.M., Liu, M., Sheng, Z.M., Murakami, M., Chen, M., Yu, L.L. & Zhang, J. (2016). Dense blocks of energetic ions driven by multi-petawatt lasers. *Sci. Rep*. **6**, 22150.

Weng, S.M., Murakami, M. & Sheng, Z.M. (2015). Reducing ion energy spread in hole-boring radiation pressure acceleration by using two-ion-species targets. *Laser Part. Beams* **33**, 103–107.

Wu, F.J., Zhou, W.M., Shan, L.Q., Zhao, Z.Q., Yu, J.Q., Zhang, B., Yan, Y.H., Zhang, Z.M. & Gu, Y.Q. (2013). Effect of inside diameter of tip on proton beam produced by intense laser pulse on double-layer cone targets. *Laser Part. Beams* **31**, 123–127.

Yan, X.Q., Lin, C., Sheng, Z.M., Guo, Z.Y., Liu, B.C., Lu, Y.R., Fang, J.X. & Chen, J.E. (2008). Generating high-current monoenergetic proton beams by a circularly polarized laser pulse in the phase-stable acceleration regime. *Phys. Rev. Lett*. **100**, 135003.

Yu, T.P., Pukhov, A., Shvets, G. & Chen, M. (2010). Stable laser-driven proton beam acceleration from a two-ion-species ultrathin foil. *Phys. Rev. Lett*. **105**, 065002.

Zhang, X.M., Shen, B.F., Ji, L.L., Wang, W.P., Xu, J.C., Yu, Y.H. & Wang, X.F. (2011). Instabilities in interaction of circularly polarized laser pulse and overdense target. *Phys. Plasma* **18**, 073101.

Zhang, Z.M., Zhang, B., Hong, W., Yu, M.Y., Teng, J., He, S.K. & Gu, Y.Q. (2014). Envelop matching for enhanced backward Raman amplification by using self-ionizing plasmas. *Phys. Plasma* **21**, 123109.

Zhou, W.M., Gu, Y.Q., Hong, W., Cao, L.F., Zhao, Z.Q., Ding, Y.K., Zhang, B.H., Cai, H.B. & Mima, K. (2010). Enhancement of monoenergetic proton beams via cone substrate in high intensity laser pulse–double layer target interactions. *Laser Part. Beams* **28**, 585–590.